

# 1 Title: Population clustering of structural brain aging and its association with 2 brain development

3  
4 **Authors:** Haojing Duan<sup>1,2</sup>, Runye Shi<sup>3</sup>, Jujiao Kang<sup>1,2</sup>, Tobias Banaschewski<sup>4</sup>, Arun L. W.  
5 Bokde<sup>5</sup>, Christian Büchel<sup>6</sup>, Sylvane Desrivieres<sup>7</sup>, Herta Flor<sup>8,9</sup>, Antoine Grigis<sup>10</sup>, Hugh  
6 Garavan<sup>11</sup>, Penny A. Gowland<sup>12</sup>, Andreas Heinz<sup>13</sup>, Rüdiger Brühl<sup>14</sup>, Jean-Luc Martinot<sup>15</sup>,  
7 Marie-Laure Paillère Martinot<sup>16</sup>, Eric Artiges<sup>17</sup>, Frauke Nees<sup>4,8,18</sup>, Dimitri Papadopoulos  
8 Orfanos<sup>10</sup>, Tomáš Paus<sup>19,20</sup>, Luise Poustka<sup>21</sup>, Sarah Hohmann<sup>4</sup>, Nathalie Holz<sup>4</sup>, Juliane H.  
9 Fröhner<sup>22</sup>, Michael N. Smolka<sup>22</sup>, Nilakshi Vaidya<sup>23</sup>, Henrik Walter<sup>13</sup>, Robert Whelan<sup>24</sup>,  
10 Gunter Schumann<sup>1,23,25,26</sup>, Xiaolei Lin<sup>3,27\*</sup>, Jianfeng Feng<sup>1,2,3,28,29\*</sup>, IMAGEN consortium

## 11 Affiliations:

12 <sup>1</sup> Institute of Science and Technology for Brain-Inspired Intelligence, Fudan University, Shanghai, China

13 <sup>2</sup> Key Laboratory of Computational Neuroscience and Brain-Inspired Intelligence (Fudan University),  
14 Ministry of Education, China

15 <sup>3</sup> School of Data Science, Fudan University, Shanghai, China

16 <sup>4</sup> Department of Child and Adolescent Psychiatry and Psychotherapy, Central Institute of Mental Health,  
17 Medical Faculty Mannheim, Heidelberg University, Square J5, 68159 Mannheim, Germany

18 <sup>5</sup> Discipline of Psychiatry, School of Medicine and Trinity College Institute of Neuroscience, Trinity  
19 College Dublin, Dublin, Ireland

20 <sup>6</sup> University Medical Centre Hamburg-Eppendorf, Hamburg, Germany

21 <sup>7</sup> Social Genetic and Developmental Psychiatry Centre, Institute of Psychiatry, Psychology and  
22 Neuroscience, King's College London, London, UK

23 <sup>8</sup> Institute of Cognitive and Clinical Neuroscience, Central Institute of Mental Health, Medical Faculty  
24 Mannheim, Heidelberg University, Square J5, Mannheim, Germany

25 <sup>9</sup> Department of Psychology, School of Social Sciences, University of Mannheim, 68131 Mannheim,  
26 Germany

27 <sup>10</sup> NeuroSpin, CEA, Université Paris-Saclay, F-91191 Gif-sur-Yvette, France

28 <sup>11</sup> Departments of Psychiatry and Psychology, University of Vermont, 05405 Burlington, Vermont, USA

29 <sup>12</sup> Sir Peter Mansfield Imaging Centre School of Physics and Astronomy, University of Nottingham,  
30 University Park, Nottingham, United Kingdom

31 <sup>13</sup> Department of Psychiatry and Psychotherapy CCM, Charité – Universitätsmedizin Berlin, corporate  
32 member of Freie Universität Berlin, Humboldt-Universität zu Berlin, and Berlin Institute of Health, Berlin,  
33 Germany

34 <sup>14</sup> Physikalisch-Technische Bundesanstalt (PTB), Braunschweig and Berlin, Germany

35 <sup>15</sup> Institut National de la Santé et de la Recherche Médicale, INSERM U A10 "Trajectoires  
36 développementales en psychiatrie"; Université Paris-Saclay, Ecole Normale supérieure Paris-Saclay,  
37 CNRS, Centre Borelli; Gif-sur-Yvette, France

38 <sup>16</sup> Institut National de la Santé et de la Recherche Médicale, INSERM U A10 "Trajectoires  
39 développementales & psychiatrie", University Paris-Saclay, Ecole Normale Supérieure Paris-Saclay,  
40 CNRS; Centre Borelli, Gif-sur-Yvette, France; and AP-HP. Sorbonne Université, Department of Child and  
41 Adolescent Psychiatry, Pitié-Salpêtrière Hospital, Paris, France

42 <sup>17</sup> Institut National de la Santé et de la Recherche Médicale, INSERM U A10 "Trajectoires

43 **NOTE:** This preprint reports new research that has not been certified by peer review and should not be used to guide clinical practice.  
développementales en psychiatrie"; Université Paris-Saclay, Ecole Normale supérieure Paris-Saclay,

44 CNRS, Centre Borelli, Gif-sur-Yvette; and Psychiatry Department, EPS Barthélemy Durand, Etampes,  
45 France  
46 <sup>18</sup> Institute of Medical Psychology and Medical Sociology, University Medical Center Schleswig-Holstein  
47 Kiel University, Kiel, Germany  
48 <sup>19</sup> Department of Psychiatry, Faculty of Medicine and Centre Hospitalier Universitaire Sainte-Justine,  
49 University of Montreal, Montreal, Quebec, Canada  
50 <sup>20</sup> Departments of Psychiatry and Psychology, University of Toronto, Toronto, Ontario, Canada  
51 <sup>21</sup> Department of Child and Adolescent Psychiatry and Psychotherapy, University Medical Centre  
52 Göttingen, von-Siebold-Str. 5, 37075, Göttingen, Germany  
53 <sup>22</sup> Department of Psychiatry and Neuroimaging Center, Technische Universität Dresden, Dresden,  
54 Germany  
55 <sup>23</sup> Department of Psychiatry and Neurosciences, Charité–Universitätsmedizin Berlin, corporate member of  
56 Freie Universität Berlin/Humboldt-Universität zu Berlin, and Berlin Institute of Health, Berlin, Germany  
57 <sup>24</sup> School of Psychology and Global Brain Health Institute, Trinity College Dublin, Ireland  
58 <sup>25</sup> Centre for Population Neuroscience and Stratified Medicine (PONS Centre), ISTBI, Fudan University,  
59 Shanghai, China  
60 <sup>26</sup> Centre for Population Neuroscience and Stratified Medicine (PONS), Department of Psychiatry and  
61 Psychotherapy, Charité Universitätsmedizin Berlin, Germany  
62 <sup>27</sup> Huashan Institute of Medicine, Huashan Hospital affiliated to Fudan University, Shanghai, China  
63 <sup>28</sup> MOE Frontiers Center for Brain Science, Fudan University, Shanghai, China  
64 <sup>29</sup> Zhangjiang Fudan International Innovation Center, Shanghai, China  
65  
66 \* Correspondence authors.  
67 Xiaolei Lin (Address: School of Data Science, Fudan University, Shanghai, 200433, China. Email:  
68 [xiaoleilin@fudan.edu.cn](mailto:xiaoleilin@fudan.edu.cn))  
69 or  
70 Jianfeng Feng (Address: Institute of Science and Technology for Brain-inspired Intelligence, Fudan  
71 University, Shanghai, 200433, China. Email: [jianfeng64@gmail.com](mailto:jianfeng64@gmail.com))

72 **Abstract**

73 Structural brain aging has demonstrated strong inter-individual heterogeneity and mirroring  
74 patterns with brain development. However, due to the lack of large-scale longitudinal  
75 neuroimaging studies, most of the existing research focused on the cross-sectional changes of  
76 brain aging. In this investigation, we present a data-driven approach that incorporate both cross-  
77 sectional changes and longitudinal trajectories of structural brain aging and identified two brain  
78 aging patterns among 37,013 healthy participants from UK Biobank. Participants with  
79 accelerated brain aging also demonstrated accelerated biological aging, cognitive decline and  
80 increased genetic susceptibilities to major neuropsychiatric disorders. Further, by integrating  
81 longitudinal neuroimaging studies from a multi-center adolescent cohort, we validated the “last  
82 in, first out” mirroring hypothesis and identified brain regions with manifested mirroring  
83 patterns between brain aging and brain development. Genomic analyses revealed risk loci and  
84 genes contributing to accelerated brain aging and delayed brain development, providing  
85 molecular basis for elucidating the biological mechanisms underlying brain aging and related  
86 disorders.

## 87 **Introduction**

88 The structure of the brain undergoes continual changes throughout the entire lifespan, with  
89 structural brain alterations intimately linking brain development and brain aging<sup>1,2</sup>. Brain aging  
90 is a progressive process that often co-occurs with biological aging and declines of cognitive  
91 functions<sup>3-5</sup>, which contribute to the onset and acceleration of neurodegenerative<sup>6</sup> and  
92 neuropsychiatric disorders<sup>7</sup>. Studies on healthy brain aging have revealed significant inter-  
93 individual heterogeneity in the patterns of neuroanatomical changes<sup>8,9</sup>. Therefore, examining  
94 the patterns of structural brain aging and its associations with cognitive decline is of paramount  
95 importance in understanding the diverse biological mechanisms of age-related  
96 neuropsychiatric disorders.

97 Despite the fact that there exist large differences between brain development and brain  
98 aging<sup>10</sup>, a discernible association between these two processes remains evident. Direct  
99 comparisons of brain development and brain aging using structural MRI indicated a “last in,  
100 first out” mirroring pattern, where brain regions develop relatively late during adolescence  
101 demonstrated accelerated degeneration in older ages<sup>11,12</sup>. In addition, brain regions with strong  
102 mirroring effects showed increased vulnerability to neurodegenerative and neuropsychiatric  
103 disorders, including Alzheimer’s disease and schizophrenia<sup>13</sup>. However, due to the lack of  
104 large-scale longitudinal MRI studies during adolescence and mid-to-late adulthood, validation  
105 of the “last in, first out” mirroring hypothesis remains unavailable.

106 Prior investigations have largely focused on regional and cross-sectional changes of brain  
107 aging<sup>9,13,14</sup>, with relatively few studies exploring longitudinal trajectories of brain aging and its  
108 associations with brain development<sup>8,15,16</sup>. In this article, we present a data-driven approach to  
109 examine the population clustering of longitudinal brain aging trajectories using structure MRI  
110 data obtained from 37,013 healthy individuals during mid-to-late adulthood (44-82 years), and  
111 explore its association with biological aging, cognitive decline and susceptibilities for  
112 neuropsychiatric disorders. Further, mirroring patterns between longitudinal brain  
113 development and brain aging are investigated by comparing the region-specific aging /  
114 developmental trajectories, and manifestation of the mirroring patterns are investigated across  
115 the whole-brain and among participants with different brain aging patterns. Genomic analyses

116 are conducted to reveal risk loci and genes associated with accelerated brain aging and delayed  
117 brain development.

118

## 119 **Results**

### 120 **Longitudinal trajectories of whole-brain grey matter volume in mid-to-late adulthood** 121 **define two brain aging patterns.**

122 Fig. 1 provides the data sources, analytical workflow and research methodology of this study.  
123 After the sample selection process (Supplementary Fig. 1, Supplementary Tables 1 and 2),  
124 longitudinal grey matter volume (GMV) trajectories in 40 ROIs (33 cortical and 7 subcortical  
125 ROIs, see Supplementary Table 3) were estimated for each of the 37,013 healthy participants  
126 in UK Biobank. The first 15 principal components derived from dimensionality reduction via  
127 principal component analysis were used in the clustering analysis (see Methods)<sup>17,18</sup>. Two brain  
128 aging patterns were identified, where 18,929 (51.1%) participants with the first brain aging  
129 pattern (pattern 1) had higher total GMV at baseline and a slower rate of GMV decrease over  
130 time, and the remaining participants with the second pattern (pattern 2) had lower total GMV  
131 at baseline and a faster rate of GMV decrease (Fig. 2a). Comparing the region-specific rate of  
132 GMV decrease, pattern 2 showed a more rapid GMV decrease in medial occipital (lingual gyrus,  
133 cuneus and pericalcarine cortex) and medial temporal (entorhinal cortex, parahippocampal  
134 gyrus) regions (Fig. 2b, c and Supplementary Fig. 2), which had the largest loadings in the  
135 second and third principal components (Supplementary Table 4). These two patterns can be  
136 clearly stratified by both linear and non-linear dimensionality reduction methods, indicating  
137 distinct structural differences in brain aging between patterns (Supplementary Fig. 3). Sample  
138 characteristics of these 37,013 UK Biobank participants stratified by brain aging patterns are  
139 summarized in Supplementary Table 5. Overall, participants with different brain aging patterns  
140 had similar distributions with regard to age, sex, ethnicity, smoking status, Townsend  
141 deprivation index (TDI), body mass index (BMI) and years of schooling.

142

143 **Brain aging patterns were significantly associated with biological aging.**

144 To explore the relationships between structural brain aging and biological aging, we  
145 investigated the distribution of aging biomarkers, such as telomere length and PhenoAge<sup>19</sup>,  
146 across brain aging patterns identified above (Fig. 3 and Supplementary Table 6). Compared to  
147 pattern 1, participants in pattern 2 with more rapid GMV decrease had shorter leucocyte  
148 telomere length ( $P = 0.009$ , Cohen's  $D = -0.028$ ) and this association remained consistent after  
149 adjusting for sex, age, ethnic, BMI, smoking status and alcohol intake frequency<sup>20</sup>. Next, we  
150 examined PhenoAge, which was developed as an aging biomarker incorporating composite  
151 clinical and biochemical data<sup>19</sup>, and observed higher PhenoAge among participants with brain  
152 aging pattern 2 compared to pattern 1 ( $P = 0.019$ , Cohen's  $D = 0.027$ ). Again, the association  
153 remained significant after adjusting for sex, age, ethnic, BMI, smoking status, alcohol intake  
154 frequency and education years ( $P = 3.05 \times 10^{-15}$ , Cohen's  $D = 0.092$ ). Group differences in  
155 terms of each individual component of PhenoAge (including albumin, creatinine, glucose, c-  
156 reactive protein, lymphocytes percentage, mean corpuscular volume, erythrocyte distribution  
157 width, alkaline phosphatase and leukocyte count) were also investigated and results were  
158 consistent with PhenoAge (Supplementary Fig. 4).

159

160 **Accelerated brain aging was associated with cognitive decline and increased genetic**  
161 **susceptibilities to attention-deficit/hyperactivity disorder and delayed brain development.**

162 Next, we conducted comprehensive comparisons of cognitive functions between participants  
163 with different brain aging patterns. In general, those with brain aging pattern 2 (lower baseline  
164 total GMV and more rapid GMV decrease) exhibited worse cognitive performances compared  
165 to pattern 1. Specifically, brain aging pattern 2 showed lower numbers of correct pairs matching  
166 ( $P = 0.006$ , Cohen's  $D = -0.029$ ), worse prospective memory (OR = 0.943, 95% CI [0.891,  
167 0.999]), lower fluid intelligence ( $P < 1.00 \times 10^{-20}$ , Cohen's  $D = -0.102$ ), and worse numeric  
168 memory ( $P = 5.97 \times 10^{-11}$ , Cohen's  $D = -0.082$ ). No statistically significant differences were  
169 observed in terms of the reaction time ( $P = 0.99$ ) and prospective memory ( $P = 0.052$ ) between  
170 these two brain aging patterns after FDR correction. Results were consistent when using  
171 models adjusted for sex, age, and socioeconomic status (TDI, education and income)<sup>21,22</sup> (Fig.

172 4). Full results demonstrating the associations between brain aging patterns and cognitive  
173 functions are presented in Supplementary Table 7.

174 Having observed cognitive decline among participants with accelerated brain aging pattern, we  
175 next investigated whether brain aging patterns were associated with genetic vulnerability to  
176 major neuropsychiatric disorders. Since current GWAS are under-powered for attention-  
177 deficit/hyperactivity disorder (ADHD) and autism spectrum disorders (ASD) and the difficulty  
178 in identifying genetic variants was likely due to their polygenic nature, we calculated the  
179 corresponding polygenic risk scores (PRS) using multiple p value thresholds. This approach  
180 enabled robust investigation of the association between genetic susceptibility of  
181 neuropsychiatric disorders and brain imaging phenotypes. PRS for major neuro-developmental  
182 disorders including attention-deficit/hyperactivity disorder (ADHD) and autism spectrum  
183 disorders (ASD), neurodegenerative diseases including Alzheimer's disease (AD) and  
184 Parkinson's disease (PD), neuropsychiatric disorders including bipolar disorder (BIP), major  
185 depressive disorder (MDD), and schizophrenia (SCZ), and delayed structural brain  
186 development (GWAS from an unpublished longitudinal neuroimaging study)<sup>23</sup> were calculated  
187 for each participant using multiple P value thresholds (from 0.005 to 0.5 at intervals of 0.005)  
188 and results were then averaged over all thresholds (Fig. 5). The primary GWAS datasets used  
189 for calculating the PRS were listed in Supplementary Table 8. Overall, we observed increased  
190 genetic susceptibility to ADHD ( $P = 0.040$ ) and delayed brain development ( $P = 1.48 \times 10^{-6}$ )  
191 among participants with brain aging pattern 2 after FDR correction, while no statistically  
192 significant differences were observed for ASD, AD, PD, BIP, MDD and SCZ (Fig. 5). Details  
193 regarding the genetic liability to other common diseases and phenotypes using enhanced PRS  
194 from UK Biobank are displayed in Supplementary Tables 9 and 10.

195

196 **Genome Wide Association Studies (GWAS) identified significant genetic loci associated**  
197 **with accelerated brain aging.**

198 Having observed significant associations between brain aging patterns and cognitive  
199 performances / genetic liabilities to major neurodevelopmental disorders, we further  
200 investigated if there exist genetic variants contributing to individualized brain aging phenotype.

201 We conducted genome-wide association studies (GWAS) using estimated total GMV at 60  
202 years old as the phenotype. This phenotype was derived by adding individual specific  
203 deviations to the population averaged total GMV, thus providing additional information  
204 compared to studies using only cross-sectional neuroimaging phenotypes.

205 Six independent single nucleotide polymorphisms (SNPs) were identified at genome-wide  
206 significance level ( $P < 5 \times 10^{-8}$ ) (Fig. 6) and were subsequently mapped to genes using NCBI,  
207 Ensembl and UCSC Genome Browser database (Supplementary Table 11). Among them, two  
208 SNPs (rs10835187 and rs779233904) were also found to be associated with multiple brain  
209 imaging phenotypes in previous studies<sup>24</sup>, such as regional and tissue volume, cortical area and  
210 white matter tract measurements. Compared to the GWAS using global gray matter volume as  
211 the phenotype, our GWAS revealed additional signal in chromosome 7 (rs7776725), which was  
212 mapped to the intron of *FAM3C* and encodes a secreted protein involved in pancreatic cancer<sup>25</sup>  
213 and Alzheimer's disease<sup>26</sup>. This signal was further validated to be associated with specific brain  
214 aging mode by another study using a data-driven decomposition approach<sup>27</sup>. In addition,  
215 another significant loci (rs10835187,  $P = 1.11 \times 10^{-13}$ ) is an intergenic variant between gene  
216 *LGR4-AS1* and *LIN7C*, and was reported to be associated with bone density and brain volume  
217 measurement<sup>24,28</sup>. *LIN7C* encodes the Lin-7C protein, which is involved in the localization and  
218 stabilization of ion channels in polarized cells, such as neurons and epithelial cells<sup>29,30</sup>. Previous  
219 study has revealed the association of both allelic and haplotypic variations in the *LIN7C* gene  
220 with ADHD<sup>31</sup>.

221

### 222 **Mirroring patterns between brain aging and brain development.**

223 Having observed significant associations between brain aging and genetic susceptibility to  
224 neurodevelopmental disorders, we are now interested in examining the mirroring patterns  
225 between brain aging and brain development in the whole population, and whether these  
226 mirroring patterns were more pronounced in those with accelerated brain aging. Adolescents  
227 in the IMAGEN cohort showed more rapid GMV decrease in the frontal and parietal lobes,  
228 especially the frontal pole, superior frontal gyrus, rostral middle frontal gyrus, inferior parietal  
229 lobule and superior parietal lobule, while those in their mid-to-late adulthood showed more



230 accelerated GMV decrease in the temporal lobe, including medial orbitofrontal cortex, inferior  
231 parietal lobule and lateral occipital sulcus (Fig. 7a). The mirroring patterns (with slower GMV  
232 decrease during brain development and more rapid GMV decrease during brain aging) were  
233 particularly prominent in inferior temporal gyrus, caudal anterior cingulate cortex, fusiform  
234 cortex, middle temporal gyrus and rostral anterior cingulate cortex (Fig. 7b). The regional  
235 mirroring patterns became weaker when we focus on late brain aging at age 75 years old,  
236 especially in the frontal lobe and cingulate cortex. Further, mirroring patterns were represented  
237 more prominently in participants with brain aging pattern 2, where stronger mirroring between  
238 brain aging and brain development was observed in frontotemporal area, including lateral  
239 occipital sulcus and lingual gyrus (Fig. 7c).

240

#### 241 **Gene expression profiles were associated with delayed brain development and accelerated** 242 **brain aging.**

243 The Allen Human Brain Atlas (AHBA) transcriptomic dataset (<http://human.brain-map.org>)  
244 were used to obtain the spatial correlation between gene expression profiles across cortex and  
245 structural brain development/aging via partial least square (PLS) regression. The first PLS  
246 component explained 24.7% and 53.6% of the GMV change during brain development  
247 (estimated at age 15y,  $r_{\text{spearman}} = 0.51$ ,  $P_{\text{permutation}} = 0.03$ ) and brain aging (estimated at age 55y,  
248  $r_{\text{spearman}} = 0.49$ ,  $P_{\text{permutation}} = 1.5 \times 10^{-4}$ ), respectively. Seventeen of the 45 genes mapped to  
249 GWAS significant SNP were found in AHBA, with *LGR4* ( $r_{\text{spearman}} = 0.56$ ,  $P_{\text{permutation}} < 0.001$ )  
250 significantly associated with delayed brain development and *ESR1* ( $r_{\text{spearman}} = 0.53$ ,  $P_{\text{permutation}} <$   
251  $0.001$ ) and *FAM3C* ( $r_{\text{spearman}} = -0.37$ ,  $P_{\text{permutation}} = 0.004$ ) significantly associated with  
252 accelerated brain aging. *BDNF-AS* was positively associated with both delayed brain  
253 development and accelerated brain aging after spatial permutation test (Supplementary Tables  
254 12 and 13).

255 Next, we screened the genes based on their contributions and effect directions to the first  
256 PLS components in brain development and brain aging. 990 and 2293 genes were identified to  
257 be positively associated with brain development and negatively associated with brain aging at  
258 FDR corrected P value of 0.005, respectively, representing gene expressions associated with

259 delayed brain development and accelerated brain aging. These genes were then tested for  
260 enrichment of GO biological processes and KEGG pathways. Genes associated with delayed  
261 brain development showed significant enrichment in “regulation of trans-synaptic signaling”,  
262 “forebrain development”, “signal release” and “cAMP signaling pathway” (Fig. 8a), and genes  
263 associated with accelerated brain aging showed significant enrichment in “macroautophagy”,  
264 “establishment of protein localization to organelle”, “histone modification”, and “pathways of  
265 neurodegeneration – multiple diseases” (Fig. 8b). Full results of the gene set enrichment  
266 analysis were provided in Supplementary Fig. 5. In summary, the analyses from using the  
267 databases of GO biological processes and KEGG Pathways indicate synaptic transmission as  
268 an important process in the common mechanisms of brain development and aging, and cellular  
269 processes (autophagy), as well as the progression of neurodegenerative diseases, are important  
270 processes in the mechanisms of brain aging.

271

## 272 **Discussion**

273 In this study, we adopted a data-driven approach and revealed two distinct brain aging patterns  
274 using large-scale longitudinal neuroimaging data in mid-to-late adulthood. Compared to brain  
275 aging pattern 1, brain aging pattern 2 were characterized by a faster rate of GMV decrease,  
276 accelerated biological aging, cognitive decline, and genetic susceptibility to  
277 neurodevelopmental disorders. By integrating longitudinal neuroimaging data from adult and  
278 adolescent cohorts, we demonstrated the “last in, first out” mirroring patterns between  
279 structural brain aging and brain development, and showed that the mirroring pattern was  
280 manifested in the temporal lobe and among participants with accelerated brain aging. Further,  
281 genome-wide association studies identified significant genetic loci contributing to accelerated  
282 brain aging, while spatial correlation between whole-brain transcriptomic profiles and  
283 structural brain aging / development revealed important gene sets associated with both  
284 accelerated brain aging and delayed brain development.

285 Brain aging is closely related to the onset and progression of neurodegenerative and  
286 neuropsychiatric disorders. Both neurodegenerative and neuropsychiatric disorders  
287 demonstrate strong inter-individual heterogeneity, which prevents the comprehensive

288 understanding of their neuropathology and neurogenetic basis. Therefore, multidimensional  
289 investigation into disease subtyping and population clustering of structural brain aging are  
290 crucial in elucidating the sources of heterogeneity and neurophysiological basis related to the  
291 disease spectrum<sup>32</sup>. In the last decades, major developments in the subtyping of Alzheimer's  
292 disease, dementia and Parkinson's disease, have provided new perspectives regarding their  
293 clinical diagnosis, treatment, disease progression and prognostics<sup>32-34</sup>. While previous studies  
294 of brain aging mostly focused on the cross-sectional differences between cases and healthy  
295 controls, we here delineated the structural brain aging patterns among healthy participants  
296 using a novel data-driven approach that captured both cross-sectional and longitudinal  
297 trajectories of the whole-brain gray matter volume<sup>35,36</sup>. The two brain aging patterns identified  
298 using the above approach showed large differences in the rate of change in medial  
299 occipitotemporal gyrus, which is involved in vision, word processing and scene recognition<sup>37-</sup>  
300 <sup>39</sup>. Significant reduction of the gray matter volume and abnormal changes of the functional  
301 connectivity in this region were found in subjects with mild cognitive impairment (MCI) and  
302 AD, respectively<sup>40,41</sup>. Previous research on brainAGE<sup>3,42</sup> (the difference between chronological  
303 age and the age predicted by the machine learning model of brain imaging data) showed that  
304 as a biomarker of accelerated brain aging, people with older brainAGE have accelerated  
305 biological aging and early signs of cognitive decline, which is consistent with our discoveries  
306 in this study. Our results support the establishment of a network connecting brain aging patterns  
307 with biological aging profiles involving multi-organ systems throughout the body<sup>43</sup>. Since  
308 structural brain patterns might manifest and diverge decades before cognitive decline<sup>44</sup>,  
309 subtyping of brain aging patterns could aid in the early prediction of cognitive decline and  
310 severe neurodegenerative and neuropsychiatric disorders.

311 Mirroring pattern between brain development and brain aging has long been hypothesized  
312 by postulating that phylogenetically newer and ontogenetically less precocious brain structures  
313 degenerate relatively early<sup>13</sup>. Early studies have reported a positive correlation between age-  
314 related differences of cortical volumes and precedence of myelination of intracortical fibers<sup>45</sup>.  
315 Large differences in the patterns of change between adolescent late development and aging in  
316 the medial temporal cortex were previously found in studies of brain development and aging

317 patterns<sup>12</sup>. Here, we compared the annual volume change of the whole-brain gray matter during  
318 brain development and early / late stages of brain aging, and found that mirroring patterns are  
319 predominantly localized to the lateral / medial temporal cortex and the cingulate cortex. These  
320 cortical regions characterized by “last-in, first-out” mirroring patterns showed increased  
321 vulnerability to the several neuropsychiatric disorders. For example, regional deficits in the  
322 superior temporal gyrus and medial temporal lobe were observed in schizophrenia<sup>46</sup>, along with  
323 morphological abnormalities in the medial occipitotemporal gyrus<sup>47</sup>. Children diagnosed with  
324 ADHD had lower brain surface area in the frontal, cingulate, and temporal regions<sup>48</sup>. Douaud  
325 et al.<sup>13</sup> revealed a population transmodal network with lifespan trajectories characterized by the  
326 mirroring pattern of development and aging. We investigated the genetic susceptibility to  
327 individual-level mirroring patterns based on the lasting impact of neurodevelopmental genetic  
328 factors on brain<sup>15</sup>, demonstrating that those with more rapidly brain aging patterns have a  
329 higher risk of delayed development.

330 Identifying genes contributing to structural brain aging remains a critical step in  
331 understanding the molecular changes and biological mechanisms that govern age-related  
332 cognitive decline. Several genetic loci have been reported to be associated with brain aging  
333 modes and neurocognitive decline, many of which demonstrated global overlap with  
334 neuropsychiatric disorders and their related risk factors<sup>27,49,50</sup>. Here, we focused on the  
335 individual brain aging phenotype by estimating individual deviation from the population  
336 averaged total GMV and conducted genome-wide association analysis with this phenotype.  
337 Our approach identified 6 risk SNPs associated with accelerated brain aging, most of which  
338 could be further validated by previous studies using population averaged brain aging  
339 phenotypes. However, our approach revealed additional genetic signals and demonstrated  
340 genetic architecture underlying brain aging patterns overlap with bone density<sup>28,51</sup>. In addition,  
341 molecular profiling of the aging brain has been thoroughly investigated among patients with  
342 neurodegenerative diseases, but rarely conducted to shed light on the mirroring patterns among  
343 healthy participants. Analysis of the spatial correlation between gene expression profiles and  
344 structural brain development / aging further identified genes contributing to delayed brain  
345 development and accelerated brain aging. Specifically, expression of gene *BDNF-AS* was

346 significantly associated with both processes. *BDNF-AS* is an antisense RNA gene and plays a  
347 role in the pathoetiology of non-neoplastic conditions mainly through the mediation of *BDNF*<sup>52</sup>.  
348 *LGR4* (associated with delayed brain development) and *FAM3C* (associated with accelerated  
349 brain aging) identified in the spatial genetic association analysis also validated our findings in  
350 the GWAS.

351 There are several limitations in the current study that need to be addressed in future research.  
352 Firstly, the UK Biobank cohort, which we leveraged to identify population clustering of brain  
353 aging patterns, had a limited number of repeated structural MRI scans. Therefore, it remains  
354 challenging to obtain robust estimation of the longitudinal whole-brain GMV trajectory at the  
355 individual level. As a robustness check, we have calculated both intra-class correlation and  
356 variance of both random intercept and age slope to ensure appropriateness of the mixed effect  
357 models. Secondly, although aging is driven by numerous hallmarks, we have only investigated  
358 the association between brain aging patterns and biological aging in terms of telomere length  
359 and blood biochemical markers due to limitations of data access. Other dimensions of aging  
360 hallmarks and their relationship with structural brain aging need to be investigated in the future.  
361 Thirdly, our genomic analyses were restricted to "white British" participants of European  
362 ancestry. The diversity of genomic analyses will continue to improve as the sample sizes of  
363 GWAS of non-European ancestry increase. Further, although the gene expression maps from  
364 Allen Human Brain Atlas enabled us to gain insights into the spatial coupling between gene  
365 expression profiles and mirroring patterns of the brain, the strong inter-individual variation of  
366 whole-brain gene expression levels and large temporal span of the human brain samples may  
367 lead to the inaccurate correspondence in the observed associations. Finally, we focused on  
368 structural MRIs in deriving brain aging patterns in this analysis, future investigations could  
369 consider other brain imaging modalities from a multi-dimensional perspective. Nevertheless,  
370 our study represents a novel attempt for population clustering of structural brain aging and  
371 validated the mirroring pattern hypothesis by leveraging large-scale adolescent and adult  
372 cohorts.

## 373 **Methods**

374 **Participants** T1-weighted brain MRI images were obtained from 37,013 individuals aged 44-  
375 82 years old from UK Biobank (36,914 participants at baseline visit in 2014+, 4,007  
376 participants at the first follow-up visit in 2019+). All participants provided written informed  
377 consent, and ethical approval was granted by the North West Multi-Center Ethics committee  
378 (<https://www.ukbiobank.ac.uk/learn-more-about-uk-biobank/about-us/ethics>). Participants  
379 were excluded if they were diagnosed with severe psychiatric disorders or neurological  
380 diseases using ICD-10 primary and secondary diagnostic codes or from self-reported medical  
381 conditions at UK Biobank assessment center (see Supplementary Tables 1 and 2). Data were  
382 obtained under application number 19542. 1,529 adolescents with structural MRI images were  
383 drawn from the longitudinal project IMAGEN (1,463 at age 14, 1,377 at age 19 and 1,148 at  
384 age 23), of which the average number of MRI scans was 2.61 per adolescent. The IMAGEN  
385 study was approved by local ethics research committees at each research site and informed  
386 consent was given by all participants and a parent/guardian of each participant.

387  
388 **MRI acquisition** Quality-controlled T1-weighted neuroimaging data from UK Biobank and  
389 IMAGEN were processed using FreeSurfer v6.0. Detailed imaging processing pipeline can be  
390 found online for UK Biobank ([https://biobank.ctsu.ox.ac.uk/crystal/crystal/docs/brain\\_mri.pdf](https://biobank.ctsu.ox.ac.uk/crystal/crystal/docs/brain_mri.pdf))  
391 and IMAGEN ([https://github.com/imagen2/imagen\\_mri](https://github.com/imagen2/imagen_mri)). Briefly, cortical gray matter volume  
392 (GMV) from 33 regions in each hemisphere were generated using Desikan–Killiany Atlas<sup>53</sup>,  
393 and total gray matter volume (TGMV), intracranial volume (ICV) and subcortical volume were  
394 derived from ASEG atlas<sup>54</sup> (See Supplementary Table 3). Regional volume was averaged  
395 across left and right hemispheres. To avoid deficient segmentation or parcellation, participants  
396 with TGMV, ICV or regional GMV beyond 4 standard deviations from the sample mean were  
397 considered as outliers and removed from the following analyses.

398  
399 **Identification of longitudinal brain aging patterns** Whole-brain GMV trajectory was  
400 estimated for each participant in 40 brain regions of interest (ROIs) (33 cortical regions and 7  
401 subcortical regions), using mixed effect regression model with fixed linear and quadratic age

402 effects, random intercept and random age slope. Covariates include sex, assessment center,  
403 handedness, ethnic, and ICV. Models with random intercept and with both random intercept  
404 and random age slope were compared using AIC, BIC and evaluation of intra-class correlation  
405 (ICC). Results suggested that random age slope model should be chosen for almost all ROIs  
406 (Supplementary Table 14). Deviation of regional GMV from the population average was  
407 calculated for each participant at age 60 years and dimensionality reduction was conducted via  
408 principal component analysis (PCA). The first 15 principal components explaining  
409 approximately 70% of the total variations of regional GMV deviation were used in multivariate  
410 k-means clustering. Optimal number of clusters was chosen using both elbow diagram and  
411 contour coefficient (Supplementary Fig. 6). Rates of volumetric change for total gray matter  
412 and each ROI were estimated using generalized additive mixed effect models (GAMM) with  
413 fixed cubic splines of age, random intercept and random age slope, which incorporates both  
414 cross-sectional between-subject variation and longitudinal within-subject variation from  
415 40,921 observations and 37,013 participants. Covariates include sex, assessment center,  
416 handedness, ethnic, and ICV. We also applied PCA and locally linear embedding (LLE)<sup>55</sup> to  
417 the adjusted GMV ROIs in order to map the high-dimensional imaging-derived phenotypes to  
418 a low-dimensional space for stratification visualisation. The GMV of 40 ROIs at baseline were  
419 linearly adjusted for sex, assessment center, handedness, ethnic, ICV, and second-degree  
420 polynomial in age to be consistent with the whole-brain GMV trajectory model.

421

422 **Association between brain aging patterns and biological aging, cognitive decline and**  
423 **genetic susceptibilities of neuropsychiatric disorders** Individuals with Z-standardized  
424 leucocyte telomere length<sup>56</sup> and blood biochemistry (which were used to calculate PhenoAge<sup>19</sup>  
425 that characterizes biological aging) outside 4 standard deviations from the sample mean were  
426 excluded for better quality control. A total of 11 cognitive tests performed on the touchscreen  
427 questionnaire were included in the analysis. More information about the cognitive tests is  
428 provided in Supplementary Information. Comparisons of biological aging (leucocyte telomere  
429 length, PhenoAge) and cognitive function were conducted among participants with different  
430 brain aging patterns using both unadjusted and adjusted multivariate regression models with

431 Bonferroni / FDR correction. Polygenic Risk Scores (PRS) were calculated for autism spectrum  
432 disorder (ASD), attention deficit hyperactivity disorder (ADHD), Alzheimer's disease (AD),  
433 Parkinson's Disease (PD), bipolar disorder (BIP), major depressive disorder (MDD),  
434 schizophrenia (SCZ) and delayed brain development using GWAS summary statistics<sup>23</sup> at  
435 multiple P value thresholds (from 0.005 to 0.5 at intervals of 0.005, and 1), with higher P value  
436 thresholds incorporating larger number of independent SNPs. After quality control of genotype  
437 and imaging data, PRSs were generated for 25,861 participants on UK Biobank genotyping  
438 data. SNPs were pruned and clumped with a cutoff  $r^2 \geq 0.1$  within a 250 kb window. All  
439 calculations were conducted using PRSice v2.3.5<sup>57</sup>. Enhanced PRS from UK Biobank  
440 Genomics for multiple diseases were also tested. Detailed instructions for calculating enhanced  
441 PRS in UK Biobank can be found in research of Thompson et al.<sup>58</sup> Comparisons of  
442 neuropsychiatric disorders were conducted among participants with different brain aging  
443 patterns using t test with FDR correction. All statistical tests were two-sided.

444

#### 445 **Genome Wide Association Study to identify SNPs associated with brain aging patterns**

446 We performed Genome-wide association studies (GWAS) on individual deviations of total  
447 GMV relative to the population average at 60 years using PLINK 2.0<sup>59</sup>. Variants with missing  
448 call rates exceeding 5%, minor allele frequency below 0.5% and imputation INFO score less  
449 than 0.8 were filtered out after the genotyping quality control for UK Biobank Imputation V3  
450 dataset. Among the 337,138 unrelated "white British" participants of European ancestry  
451 included in our study, 25,861 with recent UK ancestry and accepted genotyping and imaging  
452 quality control were included in the GWAS. The analyses were further adjusted for age, age2,  
453 sex, assessment center, handedness, ethnic, ICV, and the first 10 genetic principal components.  
454 Genome-wide significant SNPs ( $P < 5 \times 10^{-8}$ ) obtained from the GWAS were clumped by  
455 linkage disequilibrium (LD) ( $r^2 < 0.1$  within a 250 kb window) using UKB release2b White  
456 British as the reference panel. We subsequently performed gene-based annotation in FUMA<sup>60</sup>  
457 using genome-wide significant SNPs and SNPs in close LD ( $r^2 \geq 0.1$ ) using Annotate Variation  
458 (ANNOVAR) on Ensemble v102 genes<sup>61</sup>.

459



460 **Mirroring patterns between brain aging and brain development** To validate the “last in,  
461 first out” mirroring hypothesis, we evaluated the structural association between brain  
462 development and brain aging. Longitudinal neuroimaging data from 1,529 adolescents in the  
463 IMGAEN cohort and 3,908 mid-to-late adulthood in the UK Biobank cohort were analyzed.  
464 Annual percentage volume change (APC) for each ROI was calculated among individuals with  
465 at least 2 structural MRI scans by subtracting the baseline GMV from follow-up GMV and  
466 dividing by the number of years between baseline and follow-up visits. Region-specific APC  
467 was regressed on age using smoothing spline with cross validated degree of freedom. Estimated  
468 APC for each ROI was obtained at age 15y for adolescents and at age 55y (early aging) and  
469 75y (late aging) for participants in UK Biobank. Region-specific APC during adolescence (or  
470 mid-to-late adulthood) was then standardized across all cortical regions to create the brain  
471 development (or aging) map. Finally, the brain development map and brain aging map were  
472 compared to assess the mirroring pattern for each ROI in the overall population and across  
473 different aging subgroups.

474  
475 **Gene Expression Analysis** The Allen Human Brain Atlas (AHBA) dataset  
476 (<http://human.brain-map.org>), which comprises gene expression measurements in six  
477 postmortem adults (age 24–57y) across 83 parcellated brain regions<sup>62,63</sup>, were used to identify  
478 gene expressions significantly associated with structural brain development and aging. The  
479 expression profiles of 15,633 genes were averaged across donors to form a  $83 \times 15,633$   
480 transcriptional matrix and partial least squares (PLS) regression was adopted for analyzing the  
481 association between regional change rate of gray matter volume and gene expression profiles.  
482 Specifically, estimated regional APC at 15 (obtained from IMAGEN cohort) and 55 years old  
483 (obtained from UK Biobank) were regressed on the high-dimensional gene expression profiles  
484 upon regularization. Associations between the first PLS component and estimated APC during  
485 brain development and brain aging were tested by spatial permutation analysis (10,000 times)<sup>64</sup>.  
486 Additionally, gene expression profiles of genes mapped to GWAS significant SNP were  
487 extracted from AHBA. The association between gene expression profiles of mapped genes and  
488 estimated APC during brain development and aging was also tested by spatial permutation

489 analysis. Statistical significance of each gene's contribution to the first PLS component was  
490 tested with standard error calculated using bootstrap<sup>65-67</sup>, and genes significantly associated  
491 with delayed brain development and accelerated brain aging were selected. Enrichment of  
492 Kyoto Encyclopedia of Genes and Genomes (KEGG) pathways and gene ontology (GO) of  
493 biological processes for these selected genes were analyzed using R package clusterProfiler<sup>68</sup>.  
494 All statistical significances were corrected for multiple testing using FDR.

495

## 496 **Data availability**

497 All the UK Biobank data used in the study are available at <https://www.ukbiobank.ac.uk>. The IMAGEN  
498 project data are available at <https://imagen-project.org>. GWAS summary statistics used to calculate the  
499 PRS are available in the Supplementary Table 8. Human gene expression data are available in the Allen  
500 Human Brain Atlas dataset: <https://human.brainmap.org>.

501

## 502 **Code availability**

503 R version 4.2.0 was used to perform statistical analyses. FreeSurfer version 6.0 was used to process  
504 neuroimaging data. lme4 1.1 in R version 4.2.0 was used to perform longitudinal data analyses. PRSice  
505 version 2.3.5 (<https://choishingwan.github.io/PRSice/>) was used to calculate the PRS. PLINK 2.0  
506 ([www.cog-genomics.org/plink/2.0/](http://www.cog-genomics.org/plink/2.0/)) and FUMA version 1.5.6 (<https://fuma.ctglab.nl/>) were used to  
507 perform genome-wide association analysis, and ANNOVAR was used to perform gene-based annotation.  
508 AHBA microarray expression data were processed using abagen toolbox version 0.1.3  
509 (<https://doi.org/10.5281/zenodo.5129257>). The rotate\_parcellation code used to perform a spatial  
510 permutation test of a parcellated cortical map: [https://github.com/frantisekvasa/rotate\\_parcellation](https://github.com/frantisekvasa/rotate_parcellation). Code  
511 for PLS analysis and bootstrapping to estimate PLS weights are available at  
512 [https://github.com/KirstieJane/NSPN\\_WhitakerVertes\\_PNAS2016/tree/master/SCRIPTS](https://github.com/KirstieJane/NSPN_WhitakerVertes_PNAS2016/tree/master/SCRIPTS). clusterProfiler  
513 4.6 in R version 4.2.0 was used to analyze gene-set enrichment.

## 514 References

- 515 1. Fjell, A. M. & Walhovd, K. B. Structural brain changes in aging: courses, causes and cognitive  
516 consequences. *Reviews in the Neurosciences* **21**, 187–222 (2010).
- 517 2. Shaw, P. *et al.* Neurodevelopmental trajectories of the human cerebral cortex. *Journal of neuroscience*  
518 **28**, 3586–3594 (2008).
- 519 3. Elliott, M. L. *et al.* Brain-age in midlife is associated with accelerated biological aging and cognitive  
520 decline in a longitudinal birth cohort. *Molecular psychiatry* **26**, 3829–3838 (2021).
- 521 4. Mattson, M. P. & Arumugam, T. V. Hallmarks of brain aging: adaptive and pathological modification  
522 by metabolic states. *Cell metabolism* **27**, 1176–1199 (2018).
- 523 5. Park, D. C. & Reuter-Lorenz, P. The adaptive brain: aging and neurocognitive scaffolding. *Annual*  
524 *review of psychology* **60**, 173–196 (2009).
- 525 6. Mariani, E., Polidori, M., Cherubini, A. & Mecocci, P. Oxidative stress in brain aging,  
526 neurodegenerative and vascular diseases: an overview. *Journal of Chromatography B* **827**, 65–75 (2005).
- 527 7. Kaufmann, T. *et al.* Common brain disorders are associated with heritable patterns of apparent aging  
528 of the brain. *Nature neuroscience* **22**, 1617–1623 (2019).
- 529 8. Raz, N., Ghisletta, P., Rodrigue, K. M., Kennedy, K. M. & Lindenberger, U. Trajectories of brain  
530 aging in middle-aged and older adults: regional and individual differences. *Neuroimage* **51**, 501–511  
531 (2010).
- 532 9. Raz, N. & Rodrigue, K. M. Differential aging of the brain: patterns, cognitive correlates and  
533 modifiers. *Neuroscience & Biobehavioral Reviews* **30**, 730–748 (2006).
- 534 10. Courchesne, E. *et al.* Normal brain development and aging: quantitative analysis at in vivo MR  
535 imaging in healthy volunteers. *Radiology* **216**, 672–682 (2000).
- 536 11. McGinnis, S. M., Brickhouse, M., Pascual, B. & Dickerson, B. C. Age-related changes in the  
537 thickness of cortical zones in humans. *Brain topography* **24**, 279–291 (2011).
- 538 12. Tamnes, C. K. *et al.* Brain development and aging: overlapping and unique patterns of change.  
539 *Neuroimage* **68**, 63–74 (2013).
- 540 13. Douaud, G. *et al.* A common brain network links development, aging, and vulnerability to disease.  
541 *Proc. Natl. Acad. Sci. U.S.A.* **111**, 17648–17653 (2014).
- 542 14. Suzuki, H. *et al.* Associations of regional brain structural differences with aging, modifiable risk  
543 factors for dementia, and cognitive performance. *JAMA network open* **2**, e1917257–e1917257 (2019).
- 544 15. Fjell, A. M. *et al.* Development and aging of cortical thickness correspond to genetic organization  
545 patterns. *Proceedings of the National Academy of Sciences* **112**, 15462–15467 (2015).
- 546 16. Nyberg, L. *et al.* Individual differences in brain aging: heterogeneity in cortico-hippocampal but not  
547 caudate atrophy rates. *Cerebral Cortex* **33**, 5075–5081 (2023).
- 548 17. Alexander-Bloch, A., Giedd, J. N. & Bullmore, E. Imaging structural co-variance between human  
549 brain regions. *Nature Reviews Neuroscience* **14**, 322–336 (2013).
- 550 18. Whitwell, J. L. *et al.* Distinct anatomical subtypes of the behavioural variant of frontotemporal  
551 dementia: a cluster analysis study. *Brain* **132**, 2932–2946 (2009).
- 552 19. Levine, M. E. *et al.* An epigenetic biomarker of aging for lifespan and healthspan. *Aging (alban NY)*  
553 **10**, 573 (2018).
- 554 20. Demanelis, K. *et al.* Determinants of telomere length across human tissues. *Science* **369**, eaaz6876  
555 (2020).

- 556 21. Foster, H. M. *et al.* The effect of socioeconomic deprivation on the association between an extended  
557 measurement of unhealthy lifestyle factors and health outcomes: a prospective analysis of the UK Biobank  
558 cohort. *The Lancet Public Health* **3**, e576–e585 (2018).
- 559 22. Townsend, P., Phillimore, P. & Beattie, A. *Health and Deprivation: Inequality and the North*. vol. 8  
560 (Taylor & Francis, 2023).
- 561 23. Shi, R. *et al.* Structural neurodevelopment at the individual level - a life-course investigation using  
562 ABCD, IMAGEN and UK Biobank data. *medRxiv* 2023–09 (2023).
- 563 24. Smith, S. M. *et al.* An expanded set of genome-wide association studies of brain imaging phenotypes  
564 in UK Biobank. *Nature neuroscience* **24**, 737–745 (2021).
- 565 25. Grønberg, M. *et al.* Biomarker Discovery from Pancreatic Cancer Secretome Using a Differential  
566 Proteomic Approach\* S. *Molecular & Cellular Proteomics* **5**, 157–171 (2006).
- 567 26. Liu, L., Watanabe, N., Akatsu, H. & Nishimura, M. Neuronal expression of ILEI/FAM3C and its  
568 reduction in Alzheimer’s disease. *Neuroscience* **330**, 236–246 (2016).
- 569 27. Smith, S. M. *et al.* Brain aging comprises many modes of structural and functional change with  
570 distinct genetic and biophysical associations. *elife* **9**, e52677 (2020).
- 571 28. Estrada, K. *et al.* Genome-wide meta-analysis identifies 56 bone mineral density loci and reveals 14  
572 loci associated with risk of fracture. *Nature genetics* **44**, 491–501 (2012).
- 573 29. Bohl, J., Brimer, N., Lyons, C. & Pol, S. B. V. The stardust family protein MPP7 forms a tripartite  
574 complex with LIN7 and DLG1 that regulates the stability and localization of DLG1 to cell junctions.  
575 *Journal of Biological Chemistry* **282**, 9392–9400 (2007).
- 576 30. Kaeck, S. M., Whitfield, C. W. & Kim, S. K. The LIN-2/LIN-7/LIN-10 complex mediates basolateral  
577 membrane localization of the *C. elegans* EGF receptor LET-23 in vulval epithelial cells. *Cell* **94**, 761–771  
578 (1998).
- 579 31. Lanktree, M. *et al.* Association study of brain-derived neurotrophic factor (BDNF) and LIN-7  
580 homolog (LIN-7) genes with adult attention-deficit/hyperactivity disorder. *American Journal of Medical*  
581 *Genetics Part B: Neuropsychiatric Genetics* **147**, 945–951 (2008).
- 582 32. Habes, M. *et al.* Disentangling heterogeneity in Alzheimer’s disease and related dementias using data-  
583 driven methods. *Biological psychiatry* **88**, 70–82 (2020).
- 584 33. Berg, D. *et al.* Prodromal Parkinson disease subtypes—key to understanding heterogeneity. *Nature*  
585 *Reviews Neurology* **17**, 349–361 (2021).
- 586 34. Ferreira, D., Nordberg, A. & Westman, E. Biological subtypes of Alzheimer disease: A systematic  
587 review and meta-analysis. *Neurology* **94**, 436–448 (2020).
- 588 35. Feczko, E. *et al.* The heterogeneity problem: approaches to identify psychiatric subtypes. *Trends in*  
589 *cognitive sciences* **23**, 584–601 (2019).
- 590 36. Poulakis, K. *et al.* Multi-cohort and longitudinal Bayesian clustering study of stage and subtype in  
591 Alzheimer’s disease. *Nature communications* **13**, 4566 (2022).
- 592 37. Bogousslavsky, J., Miklossy, J., Deruaz, J.-P., Assal, G. & Regli, F. Lingual and fusiform gyri in  
593 visual processing: a clinico-pathologic study of superior altitudinal hemianopia. *Journal of Neurology,*  
594 *Neurosurgery & Psychiatry* **50**, 607–614 (1987).
- 595 38. Epstein, R., Harris, A., Stanley, D. & Kanwisher, N. The parahippocampal place area: recognition,  
596 navigation, or encoding? *Neuron* **23**, 115–125 (1999).
- 597 39. Mechelli, A., Humphreys, G. W., Mayall, K., Olson, A. & Price, C. J. Differential effects of word  
598 length and visual contrast in the fusiform and lingual gyri during. *Proceedings of the Royal Society of*  
599 *London. Series B: Biological Sciences* **267**, 1909–1913 (2000).

- 600 40. Chételat, G. *et al.* Using voxel-based morphometry to map the structural changes associated with  
601 rapid conversion in MCI: a longitudinal MRI study. *Neuroimage* **27**, 934–946 (2005).
- 602 41. Yao, Z. *et al.* Abnormal cortical networks in mild cognitive impairment and Alzheimer’s disease.  
603 *PLoS computational biology* **6**, e1001006 (2010).
- 604 42. Christman, S. *et al.* Accelerated brain aging predicts impaired cognitive performance and greater  
605 disability in geriatric but not midlife adult depression. *Translational Psychiatry* **10**, 317 (2020).
- 606 43. Tian, Y. E. *et al.* Heterogeneous aging across multiple organ systems and prediction of chronic disease  
607 and mortality. *Nature Medicine* **29**, 1221–1231 (2023).
- 608 44. Aljondi, R., Szoeki, C., Steward, C., Yates, P. & Desmond, P. A decade of changes in brain volume  
609 and cognition. *Brain imaging and behavior* **13**, 554–563 (2019).
- 610 45. Raz, N. Aging of the brain and its impact on cognitive performance: Integration of structural and  
611 functional findings. (2000).
- 612 46. Honea, R., Crow, T. J., Passingham, D. & Mackay, C. E. Regional deficits in brain volume in  
613 schizophrenia: a meta-analysis of voxel-based morphometry studies. *American Journal of Psychiatry* **162**,  
614 2233–2245 (2005).
- 615 47. Schultz, C. C. *et al.* Increased parahippocampal and lingual gyrification in first-episode  
616 schizophrenia. *Schizophrenia Research* **123**, 137–144 (2010).
- 617 48. Hoogman, M. *et al.* Brain imaging of the cortex in ADHD: a coordinated analysis of large-scale  
618 clinical and population-based samples. *American Journal of Psychiatry* **176**, 531–542 (2019).
- 619 49. Glahn, D. C. *et al.* Genetic basis of neurocognitive decline and reduced white-matter integrity in  
620 normal human brain aging. *Proceedings of the National Academy of Sciences* **110**, 19006–19011 (2013).
- 621 50. Brouwer, R. M. *et al.* Genetic variants associated with longitudinal changes in brain structure across  
622 the lifespan. *Nature neuroscience* **25**, 421–432 (2022).
- 623 51. Zheng, H.-F. *et al.* Whole-genome sequencing identifies EN1 as a determinant of bone density and  
624 fracture. *Nature* **526**, 112–117 (2015).
- 625 52. Ghafouri-Fard, S., Khoshbakht, T., Taheri, M. & Ghanbari, M. A concise review on the role of BDNF-  
626 AS in human disorders. *Biomedicine & Pharmacotherapy* **142**, 112051 (2021).
- 627 53. Desikan, R. S. *et al.* An automated labeling system for subdividing the human cerebral cortex on MRI  
628 scans into gyral based regions of interest. *Neuroimage* **31**, 968–980 (2006).
- 629 54. Fischl, B. *et al.* Whole brain segmentation: automated labeling of neuroanatomical structures in the  
630 human brain. *Neuron* **33**, 341–355 (2002).
- 631 55. Roweis, S. T. & Saul, L. K. Nonlinear dimensionality reduction by locally linear embedding. *science*  
632 **290**, 2323–2326 (2000).
- 633 56. Codd, V. *et al.* Polygenic basis and biomedical consequences of telomere length variation. *Nature*  
634 *genetics* **53**, 1425–1433 (2021).
- 635 57. Choi, S. W. & O’Reilly, P. F. PRSice-2: Polygenic Risk Score software for biobank-scale data.  
636 *Gigascience* **8**, giz082 (2019).
- 637 58. Thompson, D. J. *et al.* UK Biobank release and systematic evaluation of optimised polygenic risk  
638 scores for 53 diseases and quantitative traits. *MedRxiv* 2022–06 (2022).
- 639 59. Chang, C. C. *et al.* Second-generation PLINK: rising to the challenge of larger and richer datasets.  
640 *Gigascience* **4**, s13742-015 (2015).
- 641 60. Watanabe, K., Taskesen, E., Van Bochoven, A. & Posthuma, D. Functional mapping and annotation of  
642 genetic associations with FUMA. *Nature communications* **8**, 1826 (2017).

- 643 61. Wang, K., Li, M. & Hakonarson, H. ANNOVAR: functional annotation of genetic variants from high-  
644 throughput sequencing data. *Nucleic acids research* **38**, e164–e164 (2010).
- 645 62. Hawrylycz, M. J. *et al.* An anatomically comprehensive atlas of the adult human brain transcriptome.  
646 *Nature* **489**, 391–399 (2012).
- 647 63. Markello, R. D. *et al.* Standardizing workflows in imaging transcriptomics with the abagen toolbox.  
648 *elife* **10**, e72129 (2021).
- 649 64. Váša, F. *et al.* Adolescent Tuning of Association Cortex in Human Structural Brain Networks.  
650 *Cerebral Cortex* **28**, 281–294 (2018).
- 651 65. Li, J. *et al.* Cortical structural differences in major depressive disorder correlate with cell type-specific  
652 transcriptional signatures. *Nature communications* **12**, 1647 (2021).
- 653 66. Morgan, S. E. *et al.* Cortical patterning of abnormal morphometric similarity in psychosis is  
654 associated with brain expression of schizophrenia-related genes. *Proceedings of the National Academy of*  
655 *Sciences* **116**, 9604–9609 (2019).
- 656 67. Romero-Garcia, R. *et al.* Schizotypy-related magnetization of cortex in healthy adolescence is  
657 colocated with expression of schizophrenia-related genes. *Biological psychiatry* **88**, 248–259 (2020).
- 658 68. Yu, G., Wang, L.-G., Han, Y. & He, Q.-Y. clusterProfiler: an R package for comparing biological  
659 themes among gene clusters. *Omics: a journal of integrative biology* **16**, 284–287 (2012).
- 660

## 661 **Acknowledgements**

662 This research used the UK Biobank Resource under application number 19542. We thank all  
663 participants and researchers from the UK Biobank. We thank the IMAGEN Consortium for  
664 providing the discover data. This work received support from the following sources: National  
665 Key R&D Program of China (No.2019YFA0709502), National Key R&D Program of China  
666 (No.2018YFC1312904), Shanghai Municipal Science and Technology Major Project  
667 (No.2018SHZDZX01), ZJ Lab, and Shanghai Center for Brain Science and Brain-Inspired  
668 Technology, the 111 Project (No.B18015), the European Union-funded FP6 Integrated  
669 Project IMAGEN (Reinforcement-related behaviour in normal brain function and  
670 psychopathology) (LSHM-CT- 2007-037286), the Horizon 2020 funded ERC Advanced  
671 Grant ‘STRATIFY’ (Brain network based stratification of reinforcement-related disorders)  
672 (695313), Human Brain Project (HBP SGA 2, 785907, and HBP SGA 3, 945539), the  
673 Medical Research Council Grant ‘c-VEDA’ (Consortium on Vulnerability to Externalizing  
674 Disorders and Addictions) (MR/N000390/1), the National Institute of Health (NIH)  
675 (R01DA049238, A decentralized macro and micro gene-by-environment interaction analysis  
676 of substance use behavior and its brain biomarkers), the National Institute for Health  
677 Research (NIHR) Biomedical Research Centre at South London and Maudsley NHS  
678 Foundation Trust and King’s College London, the Bundesministerium für Bildung und  
679 Forschung (BMBF grants 01GS08152; 01EV0711; Forschungsnetz AERIAL 01EE1406A,  
680 01EE1406B; Forschungsnetz IMAC-Mind 01GL1745B), the Deutsche  
681 Forschungsgemeinschaft (DFG grants SM 80/7-2, SFB 940, TRR 265, NE 1383/14-1), the  
682 Medical Research Foundation and Medical Research Council (grants MR/R00465X/1 and  
683 MR/S020306/1), the National Institutes of Health (NIH) funded ENIGMA (grants  
684 5U54EB020403-05 and 1R56AG058854-01), NSFC grant 82150710554 and European  
685 Union funded project ‘environMENTAL’, grant no: 101057429. Further support was  
686 provided by grants from: - the ANR (ANR-12-SAMA-0004, AAPG2019 - GeBra), the Eranet  
687 Neuron (AF12-NEUR0008-01 - WM2NA; and ANR-18-NEUR00002-01 - ADORe), the  
688 Fondation de France (00081242), the Fondation pour la Recherche Médicale  
689 (DPA20140629802), the Mission Interministérielle de Lutte-contre-les-Drogues-et-les-  
690 Conduites-Addictives (MILDECA), the Assistance-Publique-Hôpitaux-de-Paris and  
691 INSERM (interface grant), Paris Sud University IDEX 2012, the Fondation de l’Avenir  
692 (grant AP-RM-17-013 ), the Fédération pour la Recherche sur le Cerveau; the National  
693 Institutes of Health, Science Foundation Ireland (16/ERC/CD/3797), U.S.A. (Axon,  
694 Testosterone and Mental Health during Adolescence; RO1 MH085772-01A1) and by NIH  
695 Consortium grant U54 EB020403, supported by a cross-NIH alliance that funds Big Data to  
696 Knowledge Centres of Excellence. The funders had no role in study design, data collection  
697 and analysis, decision to publish or preparation of the manuscript.

698

## 699 **Competing interests**

700 Dr Banaschewski served in an advisory or consultancy role for eye level, Infectopharm,  
701 Lundbeck, Medice, Neurim Pharmaceuticals, Oberberg GmbH, Roche, and Takeda. He  
702 received conference support or speaker’s fee by Janssen, Medice and Takeda. He received

703 royalties from Hogrefe, Kohlhammer, CIP Medien, Oxford University Press; the present  
704 work is unrelated to these relationships. Dr Poustka served in an advisory or consultancy role  
705 for Roche and Viforpharm and received speaker's fee by Shire. She received royalties from  
706 Hogrefe, Kohlhammer and Schattauer. The present work is unrelated to the above grants and  
707 relationships. The other authors report no biomedical financial interests or potential conflicts  
708 of interest.



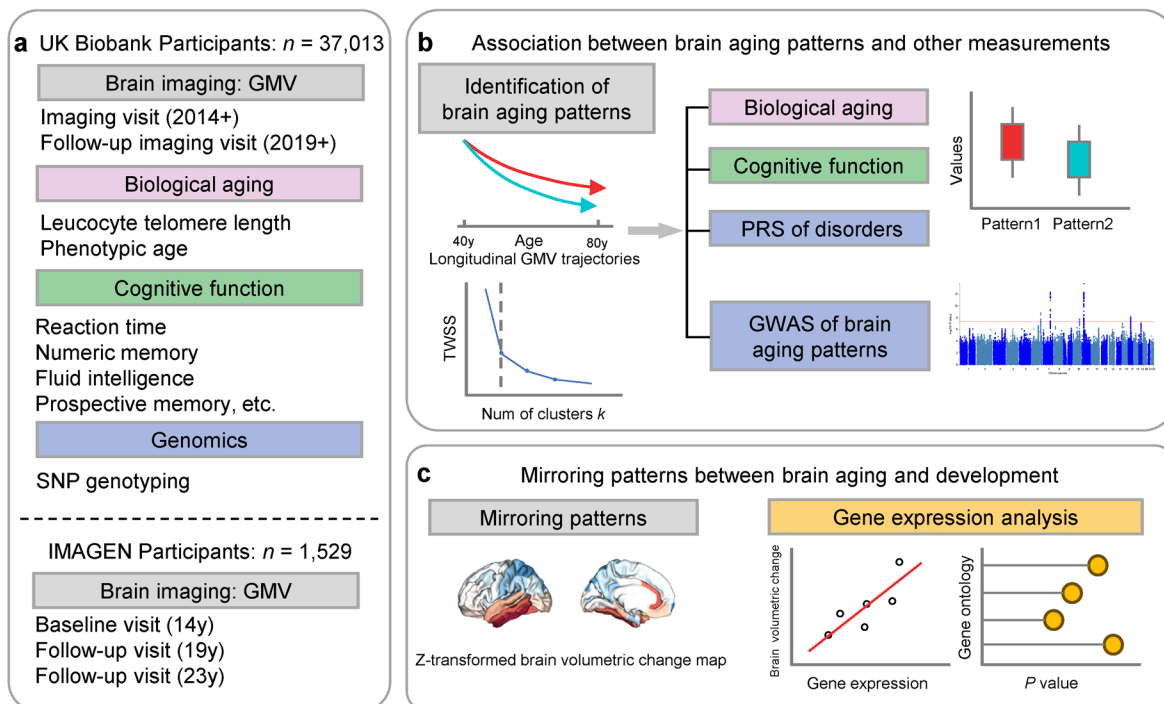


**Fig. 1 Overview of the study workflow.** **a**, Population cohorts (UK Biobank and IMAGEN) and data sources (brain imaging, biological aging biomarkers, cognitive functions, genomic data) involved in this study. **b**, Brain aging patterns were identified using longitudinal trajectories of the whole brain GMV, which enabled the capturing of long-term and individualized variations compared to only use cross-sectional data, and associations between brain aging patterns and other measurements (biological aging, cognitive functions and PRS of major neuropsychiatric disorders) were investigated. **c**, Mirroring patterns between brain aging and brain development was investigated using z-transformed brain volumetric change map and gene expression analysis.

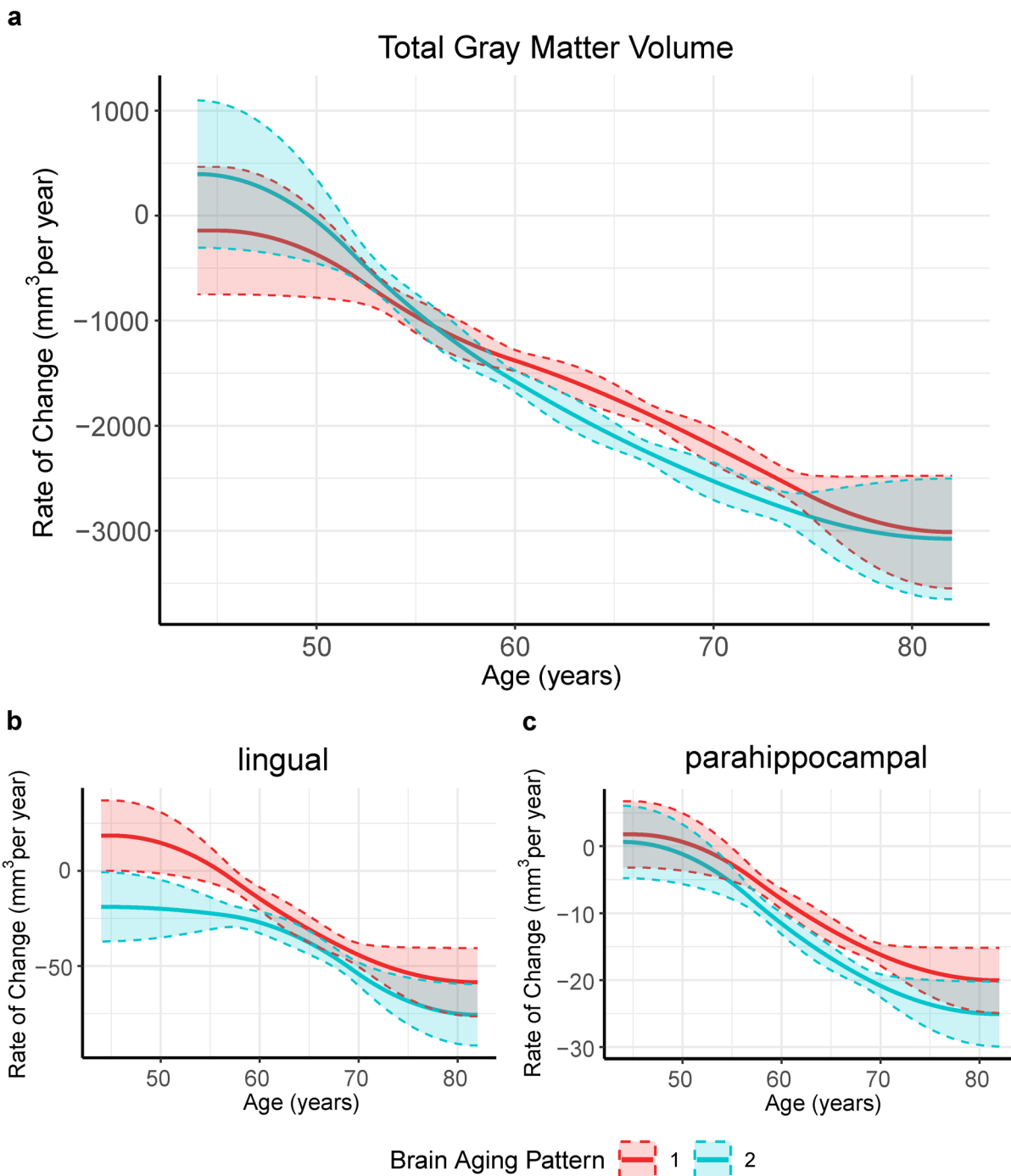


**Fig. 2 Global (a) and selected regional (b, c) cortical gray matter volume rate of change among participants with brain aging patterns 1 (red) and 2 (blue).** Rates of volumetric change for total gray matter and each ROI were estimated using GAMM, which incorporates both cross-sectional between-subject variation and longitudinal within-subject variation from 40,921 observations and 37,013 participants. Covariates include sex, assessment center, handedness, ethnic, and ICV. Shaded areas around the fit line denotes 95% CI.

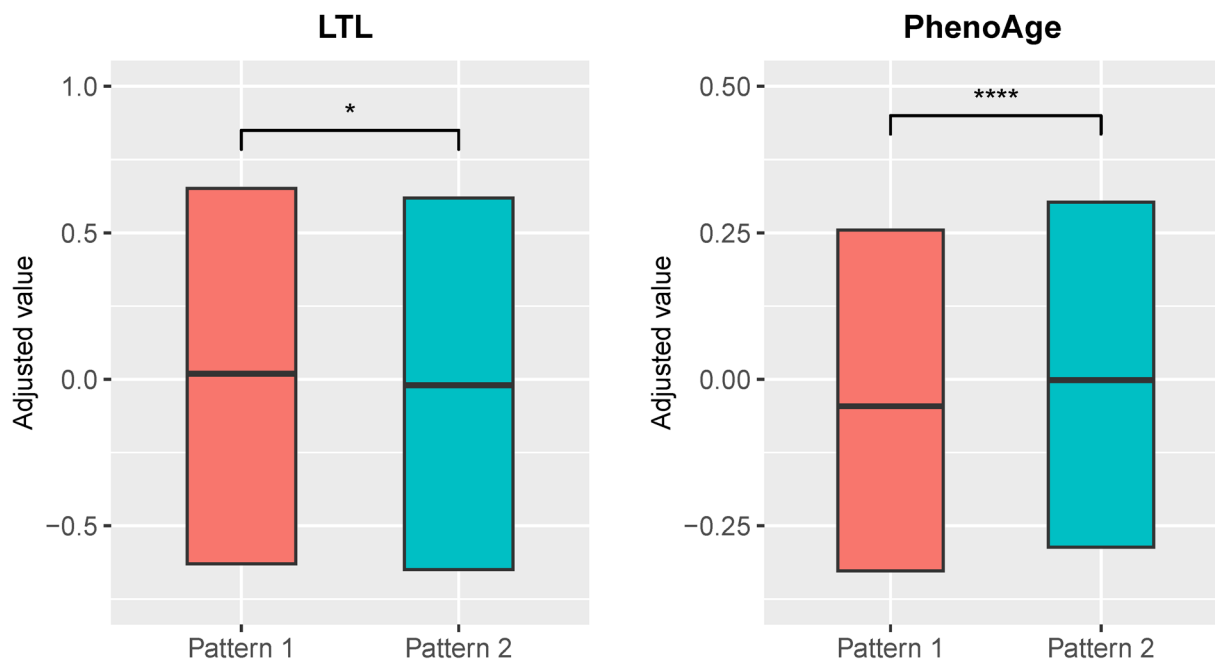


**Fig. 3 Distributions of biological aging biomarkers (leucocyte telomere length (LTL) and PhenoAge) among participants with brain aging patterns 1 and 2.** Boxes represent the interquartile range (IQR), lines within the boxes indicate the median. Two-sided P values were obtained by comparing LTL or PhenoAge<sup>19</sup> between brain aging patterns using unadjusted multivariate linear regression models. Results remained significant when adjusting for sex, age, ethnic, BMI, smoking status and alcohol intake frequency in the LTL model<sup>20</sup> and sex, age, ethnic, BMI, smoking status, alcohol frequency and education years in PhenoAge model. Stars indicate statistical significance after Bonferroni correction. \*\*\*\*:  $p \leq 0.0001$ , \*:  $p \leq 0.05$ .

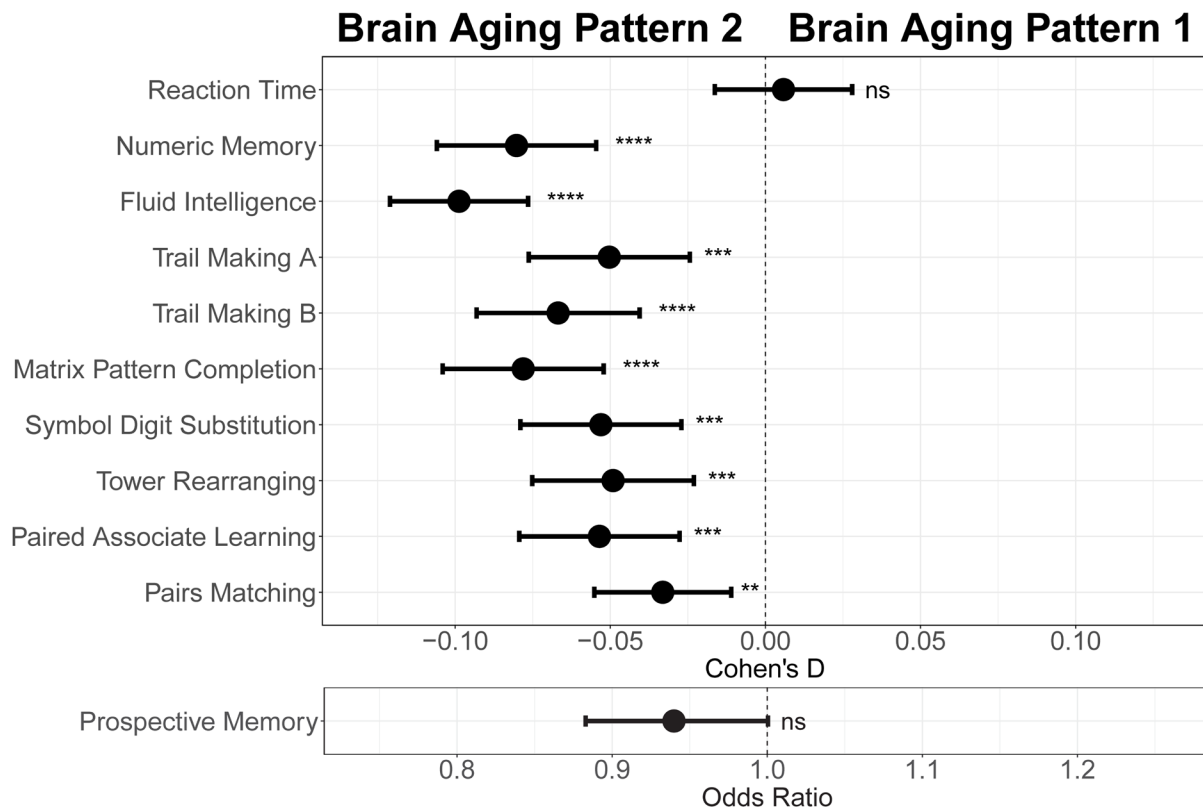


**Fig. 4 Effect size (Cohen's D or odds ratio) for comparing the cognitive functions between participants with brain aging patterns 1 and 2.** Results were adjusted such that negative Cohen's D and Odds Ratio less than 1 indicate worse cognitive performances in brain aging pattern 2 compared to pattern 1. Width of the lines extending from the center point represent 95% confidence interval. Two-sided P values were obtained using both unadjusted and adjusted (for sex, age, and TDI, education and income) multivariate regression models. Stars indicate statistical significance after FDR correction for 11 comparisons. \*\*\*\*:  $p \leq 0.0001$ , \*\*\*:  $p \leq 0.001$ , \*\*:  $p \leq 0.01$ , ns:  $p > 0.05$ .

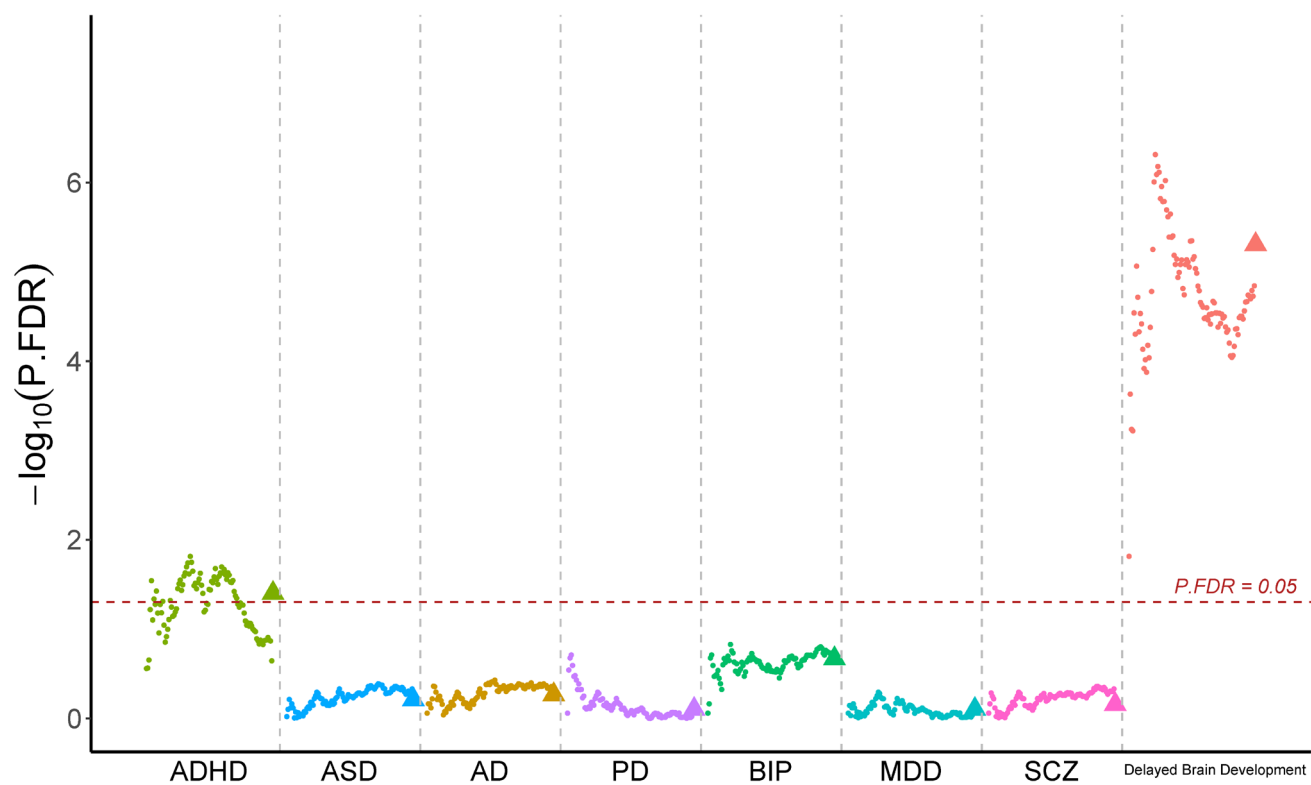


**Fig. 5 Participants with accelerated brain aging (brain aging pattern 2) had significantly increased genetic liability to ADHD and delayed brain development.** Polygenic risk score (PRS) for ADHD, ASD, AD, PD, BIP, MDD, SCZ and delayed brain development (unpublished GWAS) were calculated at different p-value thresholds from 0.005 to 0.5 at an interval of 0.005. Vertical axis represents negative logarithm of P values comparing PRS in brain aging pattern 2 relative to pattern 1. Red horizontal dashed line indicates FDR corrected P value of 0.05. Colors represent traits and dots within the same color represent different p value thresholds. The trigonometric symbol indicates the average PRS across all p-value thresholds for the same trait.

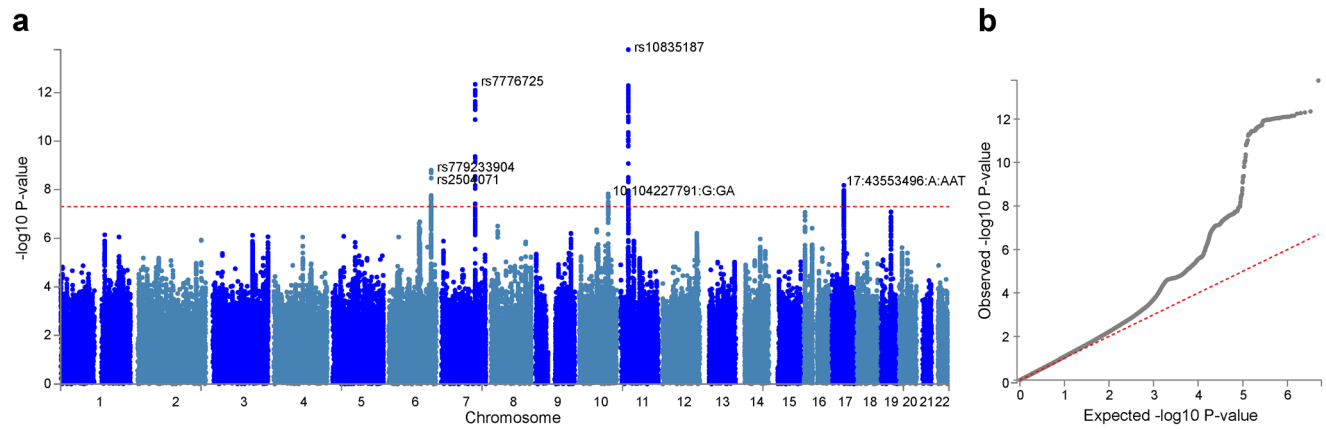


**Fig. 6 Genome-wide association study (GWAS) identified 6 independent SNPs associated with accelerated brain aging.** Total GMV at 60 years old was estimated for each participant using mixed effect models allowing for individualized baseline GMV and GMV change rate, and was used as the phenotype in the GWAS. **a**, At genome-wide significance level ( $P = 5 \times 10^{-8}$ , red dashed line), rs10835187 and rs7776725 loci were identified to be associated with accelerated brain aging. **b**, Quantile–quantile plot showed that the most significant P values deviate from the null, suggesting that results are not unduly inflated.

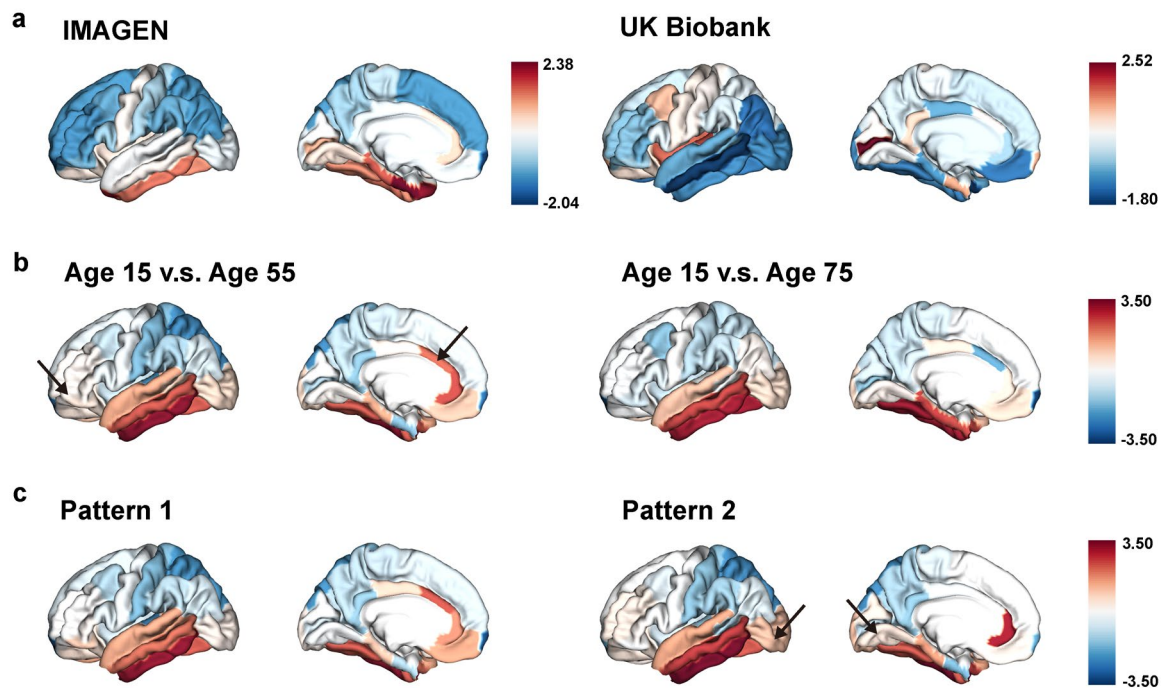


**Fig. 7 The “last in, first out” mirroring patterns between brain development and brain aging.** **a**, The annual percentage volume change (APC) was calculated for each ROI and standardized across the whole brain in adolescents (IMAGEN, left) and mid-to-late aged adults (UK Biobank, right), respectively. For adolescents, ROIs in red indicate delayed structural brain development, while for mid-to-late aged adults, ROIs in blue indicate accelerated structural brain aging. **b**, Estimated APC in brain development versus early aging (55 years old, left), and versus late aging (75 years old, right). ROIs in red indicate faster GMV decrease during brain aging and slower GMV decrease during brain development, i.e., stronger mirroring effects between brain development and brain aging. **c**, Mirroring patterns between brain development and brain aging were more manifested in participants with accelerated aging (brain aging pattern 2). The arrows point to ROIs with more pronounced mirroring patterns in each subfigure.

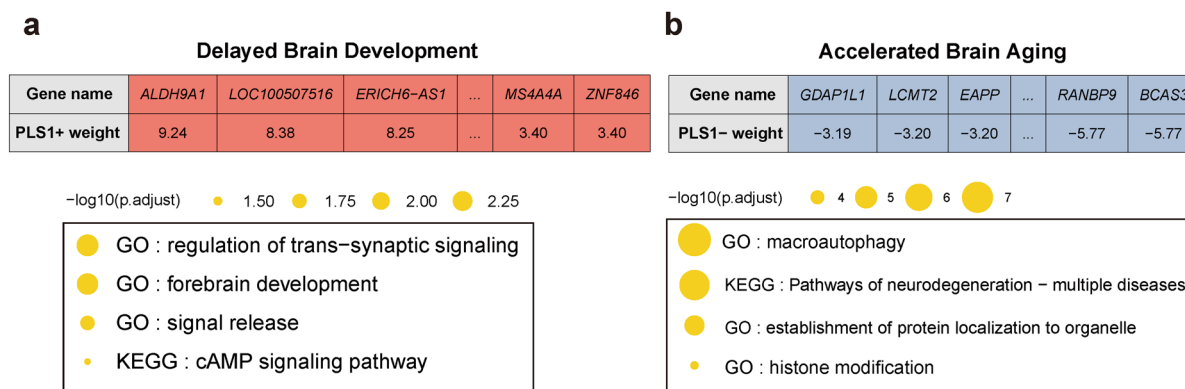


**Fig. 8 Functional enrichment of gene transcripts significantly associated with delayed brain development and accelerated brain aging.** **a**, 990 genes were spatially correlated with the first PLS component of delayed structural brain development, and were enriched for trans-synaptic signal regulation, forebrain development, signal release and cAMP signaling pathway. **b**, 2,293 genes were spatially correlated the first PLS component of accelerated structural brain aging, and were enriched for macroautophagy, pathways of neurodegeneration, establishment of protein localization to organelle and histone modification. Size of the circle represents number of genes in each term and P values were corrected using FDR for multiple comparisons.